Wave propagation in a nonlinear periodic medium

Marek Grabowski
Department of Physics, University of Colorado, Colorado Springs, Colorado 80933

Pawel Hawrylak
Division of Physics, National Research Council of Canada, Ottawa, Canada K1A 0R6
(Received 10 October 1989)

The propagation of electronic and electromagnetic waves in a periodic, nonlinear medium is described in terms of a discrete dynamical system represented by a universal, area-preserving map of a plane onto itself. The map is characterized by two control parameters: the wave vector k and the current density j. The dynamics of this Hamiltonian map is very complex admitting periodic, quasiperiodic, and chaotic orbits bifurcating and resonating at various points of the two-dimensional parameter space (k,j). The analysis of this dynamical system is based on the pattern of strong resonances and then applied to the problems of electromagnetic-wave propagation through a superlattice characterized by a strong excitonic nonlinearity and the ballistic transport of electrons in spatially periodic media.

I. INTRODUCTION

There are many very interesting phenomena associated with the propagation of electromagnetic and electronic waves in spatially periodic, nonlinear media. Recently, a number of these phenomena have been studied. In particular, Delyon *et al.*[1] have shown that a periodic modulation of a finite one-dimensional nonlinear medium induces multistability in the transmitted wave intensity, while Mills and Trullinger,[2] and Coste and Peyraud[3] have examined the localized, solitonlike structures associated with these systems. We have also studied these phenomena from the point of view of applications to the ballistic transport in semiconductor superlattices[4] and nonlinear transmission of light through multiple-quantum-well systems.[5,6] Here we shall concentrate our attention on the universal dynamics underlying these problems.

In particular, we are investigating the interplay between nonlinear effects and spatial periodicity in such materials to understand the transition from ordered (or even localized) to chaotic behavior of propagating waves. The influence of periodicity on stochastic phenomena can be emphasized by imposing discreteness on the system in the form of an array of very narrow layers of a nonlinear material embedded in a linear material. A model with these properties is proposed in Sec. II and is reminiscent of the Kronig-Penney model of solid-state physics. The δ-function periodic potential allows an easy reduction of the continuous problem to a discrete mapping of the plane onto itself, and we derive an appropriate Hamiltonian map in Sec. III, employing an interesting analogy between the wave equation and mechanical system of an isotropic harmonic oscillator periodically kicked with a nonlinear force.

The dynamics of the resulting map is then carefully examined in Sec. IV. A wide variety of behaviors ranging from the emergence of strong resonances, their growth, overlap, and ultimate destruction, to period-doubling cascades, are observed and discussed. Although many of them are already known as leading to stochasticity, new kinds of behaviors were also discovered.

We shall argue that the discrete dynamical system derived here is of general importance to the understanding of chaos in many systems such as a nonlinear Schrödinger equation, optical nonlinearities, periodically driven harmonic oscillators, and a general class of systems described by four-dimensional symplectic maps. However, only one type of these applications is discussed in detail. In Sec. V, our findings are applied to a couple of specific transmission problems, namely optical transmission through a superlattice with a nonlinear dielectric constant and transport of ballistic electrons in a tight-binding model. Finally, in the Appendix, we provide another derivation of the discrete map, trying to identify the origins of a standing controversy in the literature (compare Refs. 1 and 7 in contrast to Refs. 4–6).

II. THE WAVE EQUATION

The propagation of a stationary wave in a one-dimensional spatially periodic medium is described by a wave equation of a Schrödinger form

$$-\psi_{xx}+V(x;\psi)\psi=k^2\psi\ , \tag{1}$$

where the wave function $\Psi(x,t)=\psi(x)e^{i\omega t}+\text{c.c.}$ is time dependent with relativistic spectrum, $\omega=ck$, and the sub-

scripts x stand for spatial derivatives. The periodic modulation of a medium is modeled by an array of δ functions through a nonlinear potential

$$V(x;\psi)=2a(\mu+\alpha\psi\psi^*)\sum_n \delta(x-na) , \tag{2}$$

where a is the lattice constant, while μ and α are linear and nonlinear modulation parameters, respectively. The system described by Eqs. (1) and (2) can be physically realized by a set of very thin nonlinear layers embedded in a linear material as, for example, in semiconductor superlattices[5] or multiple quantum-well systems,[6] or by the tight-binding model for ballistic transport[4] of electrons. For realistic systems, both μ and α parameters can be wave-vector dependent reflecting, for instance, the dispersion of the nonlinear dielectric constant.

The continuous Eq. (1) can be integrated across the mth singularity, assuming continuity of the wave function $\psi(ma-0)=\psi(ma+0)\equiv\psi_m$ and a linear propagation between kicks, to obtain a discrete dynamical system,

$$\psi_{m+1}+\psi_{m-1}=2(\varepsilon+\tilde{\alpha}|\psi_m|^2)\psi m \tag{3}$$

with

$$\left.\begin{aligned}\varepsilon&=\cos(ka)+\tilde{\mu} ,\\ \left.\begin{matrix}\tilde{\mu}\\ \tilde{\alpha}\end{matrix}\right\}&=\left.\begin{matrix}\mu\\ \alpha\end{matrix}\right\}\times a^2\frac{\sin(ka)}{ka} .\end{aligned}\right. \tag{4}$$

This is just the nonlinear tight-binding Schrödinger equation previously studied[1,4] for $k=\mu=0$. It couples (ψ_{m+1},ψ_m) to (ψ_m,ψ_{m-1}) and is therefore a discrete complex map on C^2. This map, when written in terms of real and imaginary parts of ψ, can also be viewed as a measure-preserving symplectic diffeomorphism on R^4, and, as such, its dynamics is of considerable interest by itself.[8] There are additional symmetries (to be discussed shortly) of the map given by Eq. (1), which allow the reduction of dimensionality of this map from four to three[4] or even two[6] dimensions. This reduction has been incorrectly accomplished previously[1] and thus has created considerable confusion when applied to magnetic superlattice problems.[7] We shall discuss this issue in the Appendix. Here we take a different approach.

First notice that Eq. (1) can be thought of as the Euler-Lagrange equation of motion for a complex scalar field $\psi(x)$ in one dimension. The corresponding Lagrangian density can be written as

$$\mathcal{L}=\tfrac{1}{2}\{\psi_x^*\psi_x-[k^2-2\mu(x)-\alpha(x)\psi\psi^*]\psi\psi^*\} \tag{5}$$

with

$$\left.\begin{matrix}\mu(x)\\ \alpha(x)\end{matrix}\right\}=\left.\begin{matrix}\mu\\ \alpha\end{matrix}\right\}\times a\sum_n \delta(x-na) . \tag{6}$$

In the above stationary form, this model is invariant under the noncompact, unitary group U(1,1). Associated with this global gauge invariance is a conserved (divergenceless) current of which the time component is just the charge density $\psi\psi^*$, while the space component is given by the field momentum density

$$j=-\frac{i}{2}(\psi^*\psi_x-\psi\psi_x^*) . \tag{7}$$

In the continuum limit [$a\to 0$ or $\mu(x)$ and $\alpha(x)$ const], the problem is completely integrable.[9-11] For negative nonlinearity ($\alpha<0$), it possesses both soliton and soliton lattice solutions,[10,11] while for positive nonlinearity ($\alpha>0$), the model does not have a discrete spectrum (no solitons) for zero asymptotics ($k=0$) of ψ. However, for a nonzero condensate described by "chemical potential" μ, kink as well as kink-antikink lattice solutions exist,[9,11] but only for current j below a critical value.[11] Consequently, the full problem, Eqs. (5) and (6), *a priori* nonintegrable, is particularly suitable for the study of the interplay between nonlinearity and discreteness imposed by periodicity of the underlying lattice.

At this point it is useful to introduce a mechanical analog for the Lagrangian of Eq. (5) by assigning the role of time to the spatial coordinate x. Writing the complex field ψ in polar coordinates,

$$\psi(x)=A(x)e^{i\phi(x)} \tag{8}$$

and defining canonical momenta (p,j) corresponding to the amplitude A and phase ϕ degrees of freedom as

$$\left.\begin{aligned}p&\equiv A_x ,\\ j&\equiv A^2\phi_x ,\end{aligned}\right. \tag{9}$$

we obtain a two degree of freedom Hamiltonian

$$H=\frac{1}{2}\left[p^2+\left[\frac{j}{A}\right]^2+[k^2-2\mu(x)-\alpha(x)A^2]A^2\right] . \tag{10}$$

Obviously, the phase coordinate ϕ is cyclic, and thus the above Hamiltonian is effectively of a single degree of freedom, but "time" dependent with additional, "centrifugal barrier" potential. Consequently, one can interpret the Hamiltonian of Eq. (10) as describing an isotropic harmonic oscillator periodically kicked with a nonlinear force. Thus, the current j can also be viewed as the angular momentum of this oscillator.

The equations of motion resulting from the nonautonomous Hamiltonian of Eq. (10) are

$$\left.\begin{aligned}A_x&=p ,\\ p_x&=-k^2A+\frac{j^2}{A^3}+2a(\mu+\alpha A^2)A\sum_n \delta(x-na) .\end{aligned}\right. \tag{11}$$

Now let us proceed with the reduction of the above equations to a two-dimensional discrete dynamical system.

III. REDUCTION TO A DISCRETE MAP

Note that between the δ-function kicks, the equations of motion, Eqs. (11), have a solution:

$$A(x)=\left[\left[A_0\cos kx+p_0\frac{\sin(kx)}{k}\right]^2+\left[\frac{j\sin(kx)}{A_0k}\right]^2\right]^{1/2} .$$

Integration of Eq. (11) across the $(m+1)$th δ kick with $A_m \equiv A(ma+0)$, $p_m \equiv p(ma+0)$, and a continuous amplitude gives

$$A_{m+1}=\left[\left[cA_m+\frac{s}{k}p_m\right]^2+\left[\frac{J}{A_m}\right]^2\right]^{1/2},$$
$$\frac{s}{k}p_{m+1}=2(\varepsilon+\tilde{\alpha}A_{m+1}^2)A_{m+1}-cA_{m+1} \tag{12}$$
$$-\frac{A_m}{A_{m+1}}\left[cA_m+\frac{s}{k}p_m\right],$$

where $s=\sin ka$, $c=\cos ka$,

$$J=\frac{\sin(ka)}{ka}aj\ , \tag{13}$$

and ε and $\tilde{\alpha}$ are defined by Eq. (5). This two-dimensional (2D) map is area-preserving and conservative for a given value of the current j. Notice that for $j=0$, the field ψ can be taken as real, and Eqs. (12) become an amplitude-only 2D map:

$$A_{m+1}=-A_{m-1}+2(\varepsilon+\tilde{\alpha}A_m^2)A_m\ . \tag{14}$$

Since the zero-current map has already been extensively studied,[1,4] we shall concentrate on the nonzero-current problem instead.

The map given by Eqs. (12) can be further simplified by a transformation to a new pair of canonically conjugated variables

$$R=A^2,\quad Q=\frac{sp}{kA}+c\ . \tag{15}$$

Introducing a compact notation $(R_m,Q_m)\equiv(R,Q)$, $(R_{m+1},Q_{m+1})\equiv(\bar{R},\bar{Q})$, one obtains a map M, defined by

$$M:\begin{cases}\bar{R}=R\left[Q^2+\left[\frac{J}{R}\right]^2\right] & \text{(16a)}\\ \bar{Q}=2(\varepsilon+\tilde{\alpha}\bar{R})-\frac{R}{\bar{R}}Q & \text{(16b)}\end{cases}.$$

This map preserves the sign of the "charge" variable R, and is symmetric under the transformation $(\varepsilon,\tilde{\alpha},Q)\rightarrow(-\varepsilon,-\tilde{\alpha},-Q)$. Therefore, it is sufficient to study it for positive nonlinearity ($\tilde{\alpha}>0$) only, while the negative $\tilde{\alpha}$ case can be easily obtained by changing $\varepsilon\rightarrow-\varepsilon$ in the parameter space.

The fixed points of the map M are given by $Q_f=\varepsilon+\tilde{\alpha}R_f$ and the positive roots of a quartic equation

$$(\varepsilon+\tilde{\alpha}R_f)^2+\left[\frac{J}{R_f}\right]^2=1\ , \tag{17}$$

while the linear map ($\alpha=0$) has a single elliptic fixed point

$$Q_l=\varepsilon\ ,$$
$$R_l=(1-\varepsilon^2)^{-1/2}J\ . \tag{18}$$

Also, for future reference, note that the linear solution exists only for $-1<\varepsilon<1$.

Finally, for nonzero current J, it is convenient to symmetrize the map of Eqs. (16a) and (16b) shifting the momentum Q and scaling the charge R as

$$q\equiv Q-\varepsilon-r$$
$$r\equiv\tilde{\alpha}R\ , \tag{19}$$
$$\beta\equiv\tilde{\alpha}J\ .$$

The dynamics of the resulting map,

$$F:\begin{cases}\bar{r}=r(\varepsilon+r+q)^2+\beta^2/r & \text{(20a)}\\ \bar{q}=-q+(1-r/\bar{r})(\varepsilon+r+q+\bar{r}) & \text{(20b)}\end{cases}$$

is studied in the following section.

IV. DYNAMICS OF THE MAP

The dynamics of the map F is quite intricate since it depends on two parameters ε and β, while the two-dimensional Hamiltonian maps previously studied[12,13] had one-dimensional parameter space. We begin by identifying the symmetries of the map F.

The map F can be written as composition of two involutions, $F=P\circ S$, defined as

$$S:\begin{cases}\bar{r}=r & \text{(21a)}\\ \bar{q}=-q & \text{(21b)}\end{cases}$$

and

$$P:\begin{cases}\bar{r}=r(\varepsilon+r-q)^2+\beta^2/r & \text{(22a)}\\ \bar{q}=q+(1-r/\bar{r})(\varepsilon+r-q+\bar{r}) & \text{(22b)}\end{cases}.$$

Clearly, the dominant symmetry line of the map F is given by fixed points of the involution S, i.e., by the $q=0$ axis, while the complimentary symmetry is specified by the involution P, i.e., by the union of curves

$$q_\pm=\varepsilon+r\pm\sqrt{1-(\beta/r)^2}\ . \tag{23}$$

Moreover, the map F is invertible with an inverse $F^{-1}=S\circ F\circ S$.

The fixed points of the map F lie on intersections (if any) of the P- and S-symmetry lines, and thus are of the form $(r_f,0)$. Analytical expressions for those fixed points are not very illuminating since they come as solutions of a quartic equation, therefore we shall not quote them here. There are none or two fixed points—one elliptic and one hyperbolic—of the map F. For $\beta\ll1$ they can be approximately written as

$$r_e\approx(1-\varepsilon^2)^{-1/2}\beta\ ,$$
$$r_h\approx1-\varepsilon\ .$$

Their linear stability is decided[12] by the value $\mathcal{R}$ of the residue of the Jacobian determinant DF of the map:

$\mathcal{R} \equiv [2-\mathrm{tr}(DF)]/4$. When evaluated at the fixed points, this residue is given by

$$\mathcal{R}_f = 1-(\varepsilon+r_f)(\varepsilon+2r_f) \ . \tag{24}$$

The fixed orbit is stable (elliptic) for $0<\mathcal{R}_f<1$, and unstable for $\mathcal{R}_f<0$ (inversion hyperbolic) and $\mathcal{R}_f>1$ (ordinary hyperbolic).[12] As the map parameters ε and β are varied, the fixed points r_f move and their residue, Eq. (24), changes. Whenever the residue passes through one of the values

$$\mathcal{R}_f(\nu) = \sin^2(\pi/\nu) \tag{25}$$

the fixed point suffers Birkhoff multifurcation,[13] and two periodic orbits of period ν, one elliptic and one hyperbolic, are born by the fixed point. The so-called strong resonances are especially important to the study of the transition to chaos.[14] They occur at the values of the winding number $\nu=1,2,3,4$, and corresponding values of $\mathcal{R}_f=0,1,\frac{3}{4},\frac{1}{2}$. These resonant curves can easily be located in the (ε,β) parameter space of the map F. From Eqs. (17), (24), and (25) we have

$$\begin{aligned} r_{\nu\pm} &= \tfrac{1}{4}\{-3\varepsilon \pm \sqrt{\varepsilon^2+8[1-\sin^2(\pi/\nu)]}\} \ , \\ \beta^2_{\nu\pm} &= r^2_{\nu\pm}[1-(\varepsilon+r_{\nu\pm})^2] \ . \end{aligned} \tag{26}$$

The multifurcation curves of Eqs. (26) are illustrated in Fig. 1.

Based on the analysis of the strong, primary resonances, the dynamics of the map F for a fixed value of β can now be described as follows (cf. Fig. 1). For large positive values of ε there are no fixed points of the map, and thus all orbits are unbounded. As ε decreases past $\varepsilon=1$ and we cross the $(1+)$ curve of resonance $\nu=1$, two fixed points are born on the r axis of the (r,q) phase space and move apart as the symmetry line q_- of Eq. (23) shifts below the r axis. The stable elliptic fixed point moves to the left, while the unstable hyperbolic one moves to the right. Associated with the hyperbolic point is a separatrix (homoclinic orbit) which, for the values of ε close to the $(1+)$ curve, can be well approximated by the separatrix of the continuous system (i.e., the sech-like soliton solution). All orbits outside of this separatrix are unbounded, whereas those inside it are quasiperiodic and nearly integrable, resembling the soliton lattice solutions of the continuous system (see Fig. 2).

As ε decreases further, the separatrix swells in size and begins to break up into high-order periodic islands and chaotic orbits. Crossing of the $(5+)$ curve is accompanied by emergence of two period five orbits (elliptic and hyperbolic). Each has one point on the S-symmetry line and one on the P-symmetry line as seen in Fig. 2. Both orbits move radially away from the elliptic fixed point. Heteroclinic orbits connecting the five-periodic hyperbolic points quickly break up and become chaotic. Yet, for a while, they remain bounded by higher quasiperiodic orbits. As we cross the $(4+)$ of Fig. 1, both stable and unstable period-four orbits are born of the elliptic fixed point. The elliptic period-four orbit has two points on P-symmetry line, while two points of the hyperbolic orbit lie on the S-symmetry line. Again, heteroclinic orbits quickly become chaotic—bounded at first and then joining the surrounding stochastic sea.

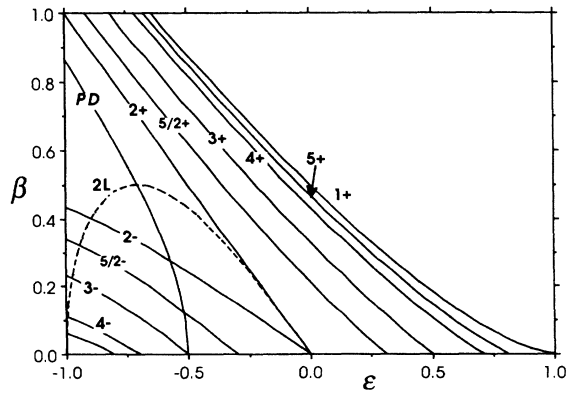

FIG. 1. Resonant curves in (ε,β) parameter space of the map F. Shown are the $\beta_{\nu\pm}$ curves of Eqs. (26), labeled $(\nu\pm)$ for $\nu=1,2,3,4$ (strong resonances) and $\nu=5,\frac{5}{2}$ (for five-periodic orbits). The curve PD marks the onset of instability of the period-two orbit while the $2L$ curve signifies the set of parameters for which the fixed point of the linear map belongs the period-two orbit of the full map.

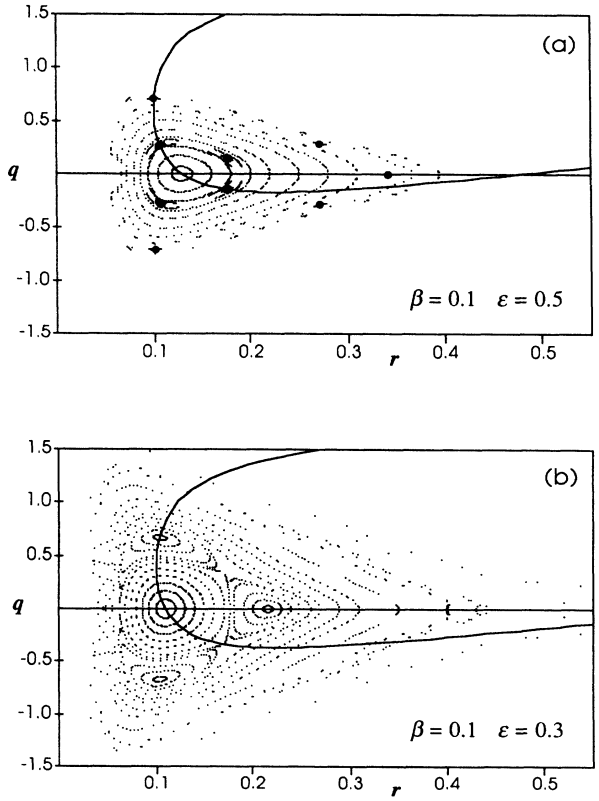

FIG. 2. The basin of stability of the elliptic fixed point of the map F for $\beta=0.1$. (a) For $\varepsilon=0.5$, narrow resonances $(5+)$ and $(4+)$ are visible as marked by solid dots. (b) For $\varepsilon=0.3$, strong resonance $(3+)$ orbits have been born out of the elliptic fixed point. On both figures, the solid line indicates the P-symmetry line.

Similarly, as we cross the (3+) curve, the elliptic fixed point gives birth to resonance-three orbits (see again Fig. 2) which in turn move away from the elliptic fixed point, then begin to overlap with higher resonances, and finally join the chaotic sea. This situation repeats itself at the $(\frac{5}{2}+)$ curve when the other resonance five is born. Furthermore, we observe that all periodic orbits follow the same rule:[12] two or no points of each even orbit and one or no points of each odd one lie on any given (*S*- or *P*-) symmetry line. This observation makes the numerical search for the periodic orbits significantly easier.

The (2+) curve of $\beta=-\varepsilon$ marks the beginning of the period-doubling (PD) cascade. At these values of the parameters, the elliptic fixed point looses its stability and hands it over to an elliptic period-two orbit (see Fig. 3). This orbit can be found analytically as

$$r_2=-\varepsilon\ ,\qquad q_2=\pm[1-(\beta/\varepsilon)^2]^{1/2}\ . \tag{27}$$

At this point, the by-now hyperbolic fixed point lies on the q_+-symmetry line of Eq. (23) and thus reverses the direction of motion along the r axis and begins to move to the right with decreasing ε. On the other hand, the two-periodic points of Eqs. (27) move along the *P*-symmetry line [cf. Eq. (23) and Fig. 2] until they loose their stability at the curve $\beta=(\varepsilon^2-\frac{1}{4})^{1/2}$ marked PD on Fig. 1. Thus the period-four elliptic orbit emerges in this second step of the period-doubling cascade. We shall not follow this route here, leaving its study to future publications, as this region of phase space is not relevant to applications discussed in the following section. Instead, we return to follow the faith of the original fixed point.

The next event takes place as we cross the (2−) curve of Fig. 1. The now-hyperbolic fixed point changes its stability again as it becomes elliptic, giving birth to a hyperbolic period-two orbit in an inverse period-doubling process (see Fig. 3). This newly born orbit is given by

$$r_{II}=\tfrac{1}{2}[-\varepsilon\pm(\varepsilon^2+2\sqrt{1-4\beta^2}-2)^{1/2}]\ ,\qquad q_{II}=0\ . \tag{28}$$

Clearly, the inverse period-doubling process preserves the symmetry of the original fixed point as the hyperbolic points stay on the *S*-symmetry line moving apart on the r axis. At the same time, the heteroclinic orbits interpolating between the hyperbolic points form a separatrix which continues to grow in size (see Fig. 3). Close to the (2−) curve, this separatrix is well approximated by the continuous system with its tanh-like kink solutions and kink-antikink lattice solutions inside the separatrix. Soon, however, the separatrix begins to break up as strong resonances emerge from the elliptic fixed point.

The "negative" resonances are formed in a sequence reversed to that of "positive" resonances described above. First, the resonance five is born at $(\frac{5}{2}-)$ curve, followed by resonance three at the (3−) curve crossing, followed by resonance four at (4−) curve of Fig. 1 and so on. The stability basins of the elliptic fixed point in the presence of resonances $(\frac{5}{2}-)$ and (3−) are illustrated in Fig. 4. The general pattern of the negative resonances' behavior is the same as for the positive resonances. Soon after formation, both stable and unstable periodic orbits move radially away from the elliptic fixed point. Their heteroclinic orbits break up and become chaotic as the resonances overlap, finally giving rise to isolated islands of stability as they join the surrounding chaotic sea. Note, however, that the specific position of periodic points belonging to negative resonances is also reversed with respect to those of positive resonances. Compare, for example, the resonance (3−) on Fig. 4 in which "triangle" of the elliptic orbit points to the left, while that of resonance (3+) of Fig. 2 points to the right: the elliptic and hyperbolic periodic orbits are exchanged for positive or negative resonances.

It should be apparent by now that the dynamics of the map F of Eqs. (20a) and (20b) has all the intricate features known from other nonlinear Hamiltonian maps.[12–14] Particularly interesting seems to be the inverse period-doubling phenomenon not found in previous studies. Its origin can be traced back to the symmetry of the map F mentioned just after Eqs. (16a) and (16b): the dynamics of the map F for positive nonlinearity differs from the

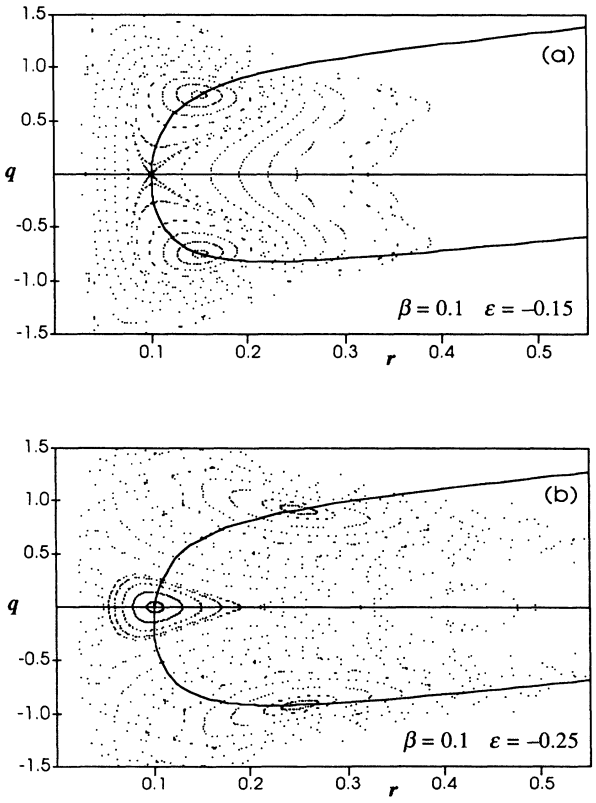

FIG. 3. The stability basins of (a) the period-two orbit of the resonance (2+) (note that the elliptic fixed point has just lost its stability) and (b) the elliptic fixed point, which regained its stability in the inverse bifurcation process. The stability islands of the (2+) resonance are still visible. The solid curve again marks the *P*-symmetry line and the (ε,β) values are noted in the corresponding panels.

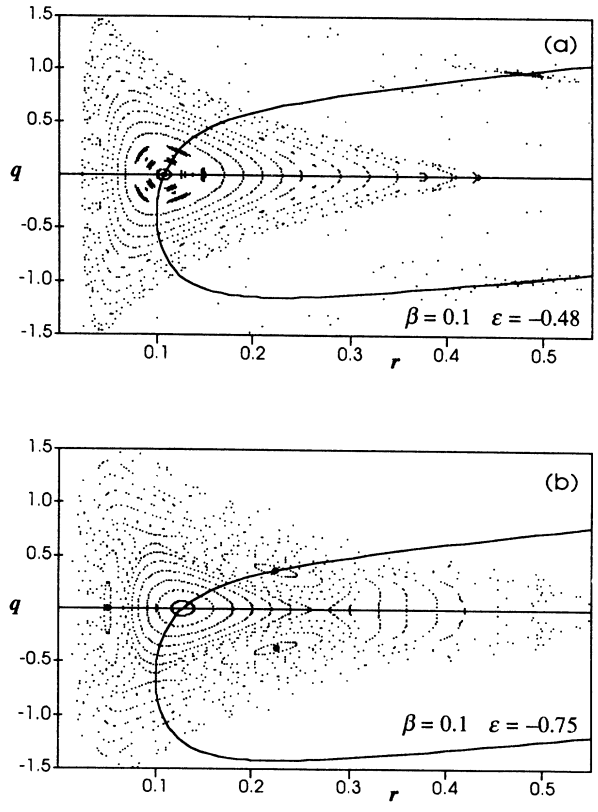

FIG. 4. The stability basin of the elliptic fixed point for $\beta=0.1$. (a) For $\varepsilon=-0.48$, i.e., soon after the emergence of the $(\frac{5}{2}-)$ resonance, most of the orbits are nearly integrable, while the period-five orbit is visible near the elliptic fixed point. Also note the spread along the P-symmetry line, barely discernible stability island of the period-two orbit around $r=0.5$. In (b) the period-three orbit of the resonance $(3-)$ is shown for $\varepsilon=-0.75$.

negative nonlinearity in that the former case the map has a "natural" hyperbolic fixed point due to a local maximum of the effective potential in the Hamiltonian of Eq. (10), while in the latter there is only a single minimum of the potential (elliptic fixed point) and the pair of hyperbolic points emerges as turning points of the potential.

The existence of the negative resonance sequence in limited parameter range implies that for values of β less than about 0.45 (cf. Fig. 1), the transition to complete chaos in our dynamical system takes place via a mechanism of primary resonances overlap, whereas for larger values of β, the elliptic fixed point does not regain its stability which it loses at $(2+)$ resonance, and the ensuing period-doubling cascade becomes the only route to chaos on the entire parameter space.

Since the dynamics of our map is so complex, we do not pretend to have a complete understanding of all its details. Nevertheless, what we have established about it so far should be sufficient to apply the map F to the description of the transmission problem which follows in the next section.

V. THE TRANSMISSION PROBLEM

Let us apply the general considerations of the preceding sections to a transmission problem defined as follows. Consider a plane, monochromatic wave of wave vector k (either electromagnetic wave or ballistic electron wave function) incident upon a spatially periodic (in x direction) nonlinear medium. If the nonlinear medium is of finite extent, this wave would be partly reflected and partly transmitted. The transmitted wave then continues to propagate as a plane wave. To determine the transmittivity of the nonlinear medium as a function of intensity and the wave vector of the incident wave, we reverse this situation, asking under what conditions the intensity of the transmitted wave remains bounded when propagated backwards.[1,4-6]

We assume that the propagating wave is described by the wave equation, Eq. (1) with Eq. (2). Consequently, in the language of the resulting map, Eqs. (16a) and (16b), or Eqs. (20a) and (20b), one can restate the general problem as follows. For a given set of parameters (a,μ,α) characterizing the medium, find a set of transmitted wave intensities T^2 and wave vectors k, for which an initial point in the phase space of the map M, or F, corresponding to the linear $(\alpha=0)$, stable fixed point of this map, belong to a bounded orbit of the map.

Now recall that the linear fixed point of the map M is given by Eqs. (18) and thus, after the rescaling of Eqs. (19), the linear fixed point of the map F is

$$r_l=(1-\varepsilon^2)^{-1/2}\beta\ ,\qquad q_l=-r_l\ . \tag{29}$$

The set of parameters (ε,β) for which an orbit of the map F originating at the initial point (r_l,q_l) remains bounded under iteration is shown in Fig. 5. The dark regions represent transmitting states. For low values of β $(\beta<0.1)$ the system is transmitting for nearly all energies ε. As β increases, several gaps in the transmission spectrum are opened and they grow in size. For larger values of β $(\beta>0.6)$, none of the states is transmitting. The origin of the gaps can be elucidated based on the analysis of

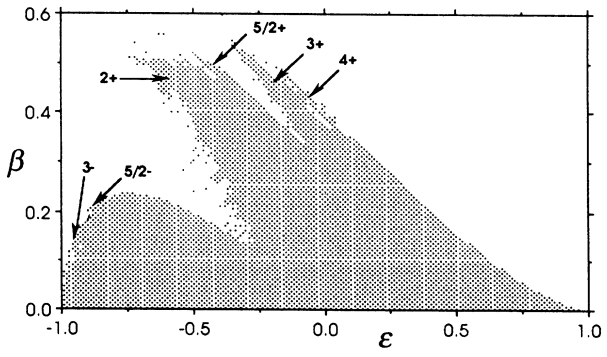

FIG. 5. The set of parameters (ε,β) for which the fixed point of the linear map (r_l,q_l) gives rise to a bound orbit under the map F. The dark tongues of this diagram are marked with resonance's indices according to the location of the initial point of the bound orbit in the corresponding stability basin of a given resonance.

the dynamics of the map F in the preceding section.

The right-most edge of the dark region of Fig. 5 can be associated with the (1+) resonance curve of Fig. 1. This is where the first bound orbits of the map F appear as contained within a rather small separatrix. Therefore, for larger values of β, the linear fixed point, Eqs. (29), falls outside the separatrix and thus generates unbounded (nontransmitting) orbits. This transition from a nontransmitting to transmitting state with decreasing ε is very sharp since, as remarked before, in the neighborhood of the (1+) resonant curve the system is nearly integrable and hence has fairly sharp separatrix. Similarly, the second sharp edge of the dark region, extending in the range of $\beta \approx 0.2$, $-0.8 < \varepsilon < -0.3$, relates to the formation of the "negative" separatrix spanned by the two-periodic hyperbolic points of the resonance (2−) (cf. Fig. 1). Again, this edge is sharp since the system is almost integrable there and has a well-defined heteroclinic orbit. As the linear fixed point crosses this orbit, there is a sharp transition to the transmitting state.

All the other dark tongues and white gaps can also be explained by referring to the analysis of the strong resonances (see, for example, the curve $2L$ of Fig. 1). In going from right to left at $\beta \approx 0.4$ of Fig. 5 the first narrow tongue encountered is identified with the linear fixed point entering, and then leaving, the stability basin of the (4+) resonance. The next, wider tongue relates to the stability basin of the (3+) resonance and is followed by a narrow resonance ($\frac{5}{2}$+) tongue. Subsequently, one encounters the largest tongue of Fig. 5 which relates to the primary resonance (2+). Similarly, moving vertically down at fixed $\varepsilon \approx -0.9$ we pass through the (barely discernible on Fig. 5) tongues of resonances ($\frac{5}{2}$−), (3−), and (4−).

The above comments explain the most apparent attributes of Fig. 5. However, then examined in more detail, this figure exhibits even more salient features. For example, all the right edges of the positive resonance tongues are sharper than the left edges. This is due to the fact that with decreasing ε the expanding resonances are catching up with the linear fixed point and, being less developed at larger ε, they have sharper boundaries. In contrast, the left edges of the tongues correspond to the by-now strongly fragmented resonances passing by and leaving the linear fixed point in the wake of stochastic layers of secondary resonances. Hence, the left edges have more structure. Particularly fragmented is the left edge of the largest (2+) resonance tongue. There the elliptic fixed point of the map F looses its stability bifurcating into a two-periodic orbit with initially large basins of stability—hence, this tongue is rather wide. However, these basins of stability quickly contract in size as the secondary resonances "eat away" the heteroclinic orbits. The surrounding phase space is full of chaotic orbits, with some of them bounded and some unbounded. Thus, in this region, the map is extremely sensitive to initial conditions and the boundary between the transmitting and nontransmitting states is very ill-defined.

Moreover, at yet smaller scale, all the boundaries of Fig. 5 are even more intricate and reveal a complex fractal structure as should be evident from Fig. 6. This structure has its origin in a complicated pattern of secondary resonances and bifurcations suffered by the elliptic points of the strong primary resonances. We shall not further investigate this matter here, leaving it to future studies.

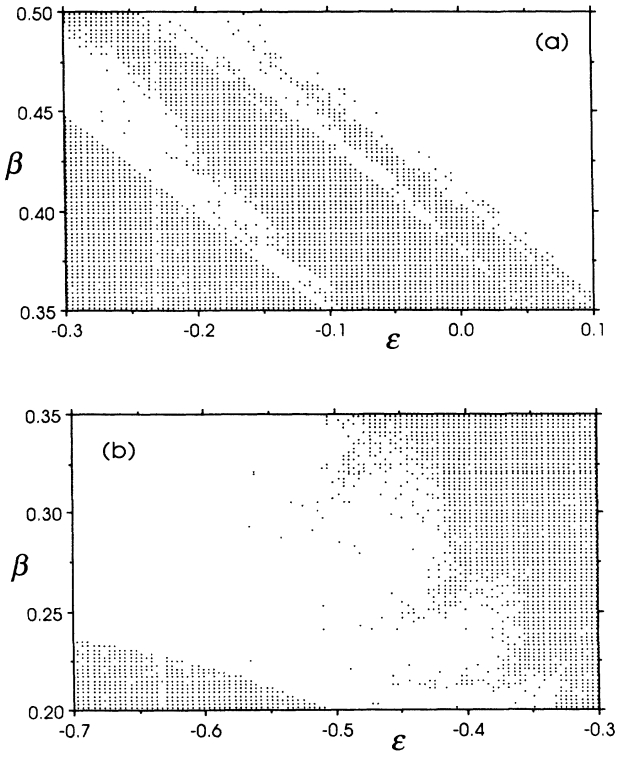

FIG. 6. Fractal structure of the transmitting states boundaries. Shown are two enlarged regions of Fig. 5: (a) the region of the (4+) and (3+) tongues and (b) interior of the largest gap between the (2+) and (2−) resonances. On both panels, a number of narrow tongues corresponding to secondary resonances can be identified.

To translate the information contained in Fig. 5 into the transmitted wave intensity versus the wave-vector dependence, one has to know how, specifically, the medium parameters, μ and α, depend on the wave vector of the incident wave. As a first example, consider a plane electromagnetic wave of wave vector k incident from vacuum upon a superlattice with nonlinear dielectric constant.[5,6] The transmitted wave is then of the form $\psi(x) = Te^{ikx}$, and the conserved current j of Eq. (7), related to the energy flow along the superlattice is $j = kT^2$, specifying the map parameter J defined in Eq. (13) as $J = \sin(ka)T^2$. If, in addition, we set $\mu = 0$ and assume that the nonlinearity parameter is wave-vector dependent[5] as $\alpha = gk^2$ we obtain from the definition of Eqs. (4) and (19),

$$\beta = ka\sqrt{1-\varepsilon^2}gT^2 \ , \varepsilon = \cos(ka) \ . \tag{30}$$

Replotting now the dark points of Fig. 5, which represent transmitting states, on the ka versus gT^2 axis set, one can reproduce Fig. 1 of Ref. 5. Subsequently, following the procedure outlined in that reference, one can establish multistability of the transmission spectrum as a function

of incident intensity. Moreover, notice that keeping the linear modulation parameter μ nonzero would allow us also to study the transmission of waves from outside of the allowed band of the linear medium.

For a second specific example we turn to the tight-binding model[1] with its application to the transport of ballistic electrons through a nonlinear superlattice.[4] Adjusting the parameters of the map F to describe this situation we note that, since the vacuum is now periodically modulated, $k=0$ in the original Eq. (1) and the plane wave in the periodically modulated medium is of the form $\psi_m = Te^{iKam}$. Thus, the discrete current, Eq. (A1), is now given as $J_m = \sin(ka)T^2$, leading to $\beta = a^2 \sin(Ka)\alpha T^2$. Moreover, requiring that the propagating waves describe electrons from the allowed band only, i.e,. with energies $\varepsilon = 1+\mu = \cos(Ka)$, the sought-after transmission diagram can be obtained from Fig. 5 in new variables,

$$a^2\alpha T^2 = \beta(1-\varepsilon^2)^{-1/2}\ , \quad \varepsilon = \cos(Ka)\ . \tag{31}$$

The resulting figure is given in Ref. 1 and thus will not be reproduced here. All the dark tongues and white gaps have their origin in the effects already discussed in the beginning of this section.

The tight-binding model of the last example, being in principle quantum mechanical, can provide an interesting bridge connecting spatial chaos phenomena of classical systems to the quantum chaos, if such exists. Again, we leave this fascinating perspective to future investigations.

ACKNOWLEDGMENTS

M. G. acknowledges partial support of the U.S. Army Research Office (A.R.O.) Grant No. DAAL03-88-K-0061, as well as the hospitality and partial support of the Microstructural Science Laboratory of the National Research Council of Canada.

APPENDIX

Here we give a different derivation of the map of Eqs. (16a) and (16b) to further clarify the relationship between the discrete, complex map of Eq. (3) and the equivalent Hamiltonian system introduced in the main text. We begin by defining three discrete variables based on the wave function ψ_m:

$$\begin{aligned} R_m &\equiv \psi_m^* \psi_m\ , \\ b_m &\equiv \tfrac{1}{2}(\psi_m^* \psi_{m+1} + \psi_{m+1}^* \psi_m)\ , \\ J_m &\equiv -\frac{i}{2}(\psi_m^* \psi_{m+1} - \psi_{m+1}^* \psi_m)\ . \end{aligned} \tag{A1}$$

Let us call R_m, b_m, and J_m the charge, bond charge, and current, respectively. It is clear from the above definitions that the following identity holds:

$$R_{m+1}R_m = b_m^2 + J_m^2\ . \tag{A2}$$

Moreover, multiplication of Eq. (3) by ψ_m^* and its complex conjugated by ψ_m and subsequent addition of the resulting equations gives

$$b_m + b_{m-1} = 2(\varepsilon + \tilde{\alpha} R_m)R_m \tag{A3}$$

while subtraction yields just current conservation $J_m = J_{m-1} = \text{const}$. Equation (A2) together with Eq. (A3) constitute a two-dimensional map for the charge and bond-charge variables. Note, however, that this map is *not area-preserving*, i.e., the charge and bond-charge variables are not canonically conjugated. To establish a one-to-one correspondence between the map defined above and the map given by Eqs. (16a) and (16b) we replace the bond charge by a new variable

$$Q_m \equiv \frac{b_m}{R_m}\ . \tag{A4}$$

The resulting map now reads

$$\begin{aligned} R_{m+1} &= R_m \left[Q_m^2 + \left[\frac{J_m}{R_m} \right]^2 \right]\ , \\ Q_{m+1} &= 2(\varepsilon + \tilde{\alpha} R_{m+1}) - \frac{R_m}{R_{m+1}} Q_m\ , \end{aligned} \tag{A5}$$

and is identical to the map of Eqs. (16a) and (16b) with discrete definitions of the canonical variables and conserved current given in Eqs. (A1) with Eq. (A4).

The maps given by Eqs. (16a) and (16b) or Eqs. (A5) cannot be reduced to a two-point map in charge variable only as done previously[1,7] by elimination of canonical momentum Q. Attempting to reduce the map of Eqs. (A5) to a form similar to that of Refs. 1 and 7 we obtain

$$\begin{aligned} R_{m+1} = R_{m-1} &+ 4(\varepsilon + \tilde{\alpha} R_m) \\ &\times [(\varepsilon + \tilde{\alpha} R_m)R_m \\ &- \operatorname{sgn}(Q_{m-1}) \sqrt{R_m R_{m-1} - J^2}]\ . \end{aligned} \tag{A6}$$

Hence, the momentum variable Q enters the map in a nontrivial way and has to be recalculated according with Eqs. (A5) at every successive step of iteration. Ignoring the $\operatorname{sgn}(Q)$ in Eq. (A6) as done in Refs. 1 and 7 leads to a map with completely *different* dynamics than that of the map described by Eqs. (16a) and (16b).

[1] François Delyon, Yves-Emmanuel Lévy, and Bernard Souillard, Phys. Rev. Lett. **57**, 2010 (1986).
[2] D. L. Mills and S. E. Trullinger, Phys. Rev. B **36**, 947 (1987).
[3] J. Coste and J. Peyraud, Phys. Rev. B **39**, 13 086 (1989).
[4] P. Hawrylak, M. Grabowski, and P. Wilson, Phys. Rev. B **40**, 6398 (1989).
[5] Pawel Hawrylak and Marek Grabowski, Phys. Rev. B **40**, 8013 (1989).
[6] Pawel Hawrylak and Marek Grabowski, Surf. Sci. (to be published).
[7] L. Kahn, N. S. Almeida, and D. L. Mills, Phys. Rev. B **37**, 8072 (1988); A. Mauger, N. S. Almeida, and D. L. Mills, *ibid.*

38, 1296 (1988).

[8]Jian-min Mao and Robert H. G. Helleman, Phys. Rev. A **35**, 1847 (1987).

[9]V. G. Makhankov and V. K. Fedyanin, Phys. Rep. **104**, 1 (1984).

[10]Piotr Garbaczewski, *Classical and Quantum Field Theory of Exactly Soluble Nonlinear Systems* (World Scientific, Singapore, 1985).

[11]Marek Grabowski (unpublished).

[12]J. M. Greene, R. S. McKay, F. Vivaldi, and M. J. Feigenbaum, Physica D (Amsterdam) **3D**, 468 (1981).

[13]Tassos C. Bountis, Physica D (Amsterdam) **3D**, 577 (1981).

[14]R. H. G. Helleman, in *Fundamental Problems in Statistical Mechanics,* edited by E. G. D. Cohen (North-Holland, Amsterdam, 1980), Vol. 5.

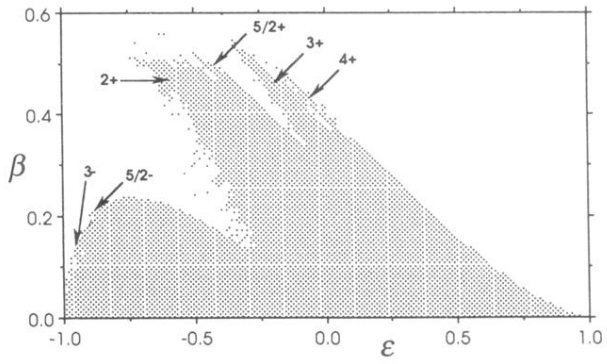

FIG. 5. The set of parameters (ε,β) for which the fixed point of the linear map (r_l,q_l) gives rise to a bound orbit under the map F. The dark tongues of this diagram are marked with resonance's indices according to the location of the initial point of the bound orbit in the corresponding stability basin of a given resonance.